Hindawi
Advances in Polymer Technology
Volume 2019, Article ID 9562437, 9 pages
https://doi.org/10.1155/2019/9562437

Research Article

Release Behavior of Folic Acid Grafted Hollow Hydroxyapatite as Drug Carrier

Qing Liu, Wenjing Guo, Mei Yang, Kejie Wang, Weijun Liu, and Fanhong Wu

School of Chemical and Environmental Engineering, Shanghai Institute of Technology, 100 Haiquan Road, Shanghai 201418, China

Correspondence should be addressed to Weijun Liu; liuwj@sit.edu.cn

Received 9 October 2018; Revised 22 January 2019; Accepted 13 February 2019; Published 4 March 2019

Academic Editor: Leandro Gurgel

Based on the formation of carbodiimide compounds between carboxyl and primary amines, hollow microspheres arising from the folic acid (folate-FA) grafted onto the surface of the modified hydroxyapatite were successfully prepared. The hollow morphology and composition of the FA-grafted hydroxyapatite microspheres were confirmed by scanning electron microscopy (SEM) and other characterizations. Brunauer-Emmett-Teller (BET) assay revealed the specific surface area and average pore size of the microspheres were 34.58m^2/g and 17.80 nm, respectively. As a drug carrier, the kinetic investigation of doxorubicin (DOX) loaded shows that the adsorbed behavior of drug on the adsorbent is more suitable to be described with pseudo-first-order model. Furthermore, the release rate can reach 83% at pH 5.7, which is greater than the release of 39% at pH 7.4, indicating an excellent performance of controlled drug release for response pH. The release mechanism of DOX coincides with Fickian diffusion as a result of Korsmeyer-Peppas model analysis and the release phenomena can be well explained by Fickian diffusion second law.

1. Introduction

In recent years, hydroxyapatite has received great attention in tissue engineering and biomedical areas due to its similarity to the mineral component of bone tissues [1–3], excellent biocompatibility [4–6], and bioactivity as well as osteoconductive feature without causing local or systemic toxicity and inflammation [7, 8]. As for the applications of biological medicine fields, the hydroxyapatite has been extensively investigated as control-released carriers of drug, such as antibiotics [9–11], 5-flurouracil [12], and protein drugs [13, 14].

As an ideal carrier of drug, good loading and control-released ability as well as the active targeting are always expected by people. Especially, as the first-line drug for a wide range of cancers, doxorubicin hydrochloride (DOX), an effective antibiotic, is usually applied to killing cancer cells or inhibiting their proliferation by means of chemotherapy way [15, 16]. However, long-term or repeated therapeutic action can create nonselective cytotoxicity because of the lack of targeted ability for cancer cells and then leads to severe side effects. In order to overcome these issues and improve therapeutic efficacy, many researchers have focused on such a kind of explorations to modify hydroxyapatite particles with specific ligands as a drug control-released carriers. It is well known that folic acid (folate–FA) is one of the receptor mediated targeting moieties [17–19] and its receptor shows an overexpression on the surfaces of cancer cells, such as breast, brain, kidney, and ovarian. Hence, the drug carriers covalently conjugated with FA could achieve selective targeting to cancer cells [20]. For the various drugs, the pathway to prepare drug carriers with the FA-modified method can be different, and the performance of the carriers obtained can also vary. Regarding the prepared process, the hydroxyapatite can be either functionalized by polyethylene glycol (PEG) in advance or directly functionalized with folic acid [21] or aminated folic acid [22], and the relevant assessments showed that these modified microparticles could be a great candidate for biomedical application. Of course, the microparticles mentioned above do not possess the hollow morphology that has been noticed.

Although the hydroxyapatites with nanoscale have attracted more attention of researchers owing to the highly specific surface area and large capacity for drug loading. But, it may be expected that the porous hollow hydroxyapatite microparticles possess greater potential as one of the

promising drug carriers based on the advantages of nano-sized hydroxyapatite. Therefore, a series of hydroxyapatite microparticles with porous structure have been prepared using a great diversity of methods or strategies, for instance, previously reported emulsion preparation [23], sol-gel synthesis [24], frequently used hydrothermal fabrication [25–27], and template method [28], as well as microwave-assistant method [29, 30] and others [31–34]. The relevant studies and characterizations have also illustrated a better performance of this kind of microparticles as drug carriers [35]. In general, for the preparation of hollow hydroxyapatite by hydrothermal approach, the vaterite $CaCO_3$ is often selected as the sacrificial template. Under the alkaline condition, the hydrated Ca^{2+} cations on the surface of the hollow $CaCO_3$ templates can react with PO_4^{3-} added into the solution and then create a replacement of CO_3^{2-} by PO_4^{3-}. As the reaction proceeds, finally, the hydroxyapatite was formed and possessed the shape and hollow structure of template microparticles. Certainly, the white $Ca(OH)_2$ emulsion can be also used as a sacrificial templates, and the shape of the as-prepared hollow hydroxyapatites retains the polyhedral structure of $Ca(OH)_2$ solid [36].

In this work, in order to explore the drug loading and release performance of FA-grafted hollow hydroxyapatite, the hollow hydroxyapatite microspheres were firstly fabricated using simple hydrothermal approach [37] and then modified the as-prepared microspheres with (3-aminopropyl)triethoxysilane (APTES) to achieve the amination for the hydroxyapatite and finally conjugate primary amines to carboxyl groups in the activated folic acid by forming carbodiimide compounds to realize the folate grafting of the modified hydroxyapatite using the related research as the basic principle [38–42]. SEM, BET, and relevant measurements characterized the morphology, porous sizes, and composition of the FA-grafted hydroxyapatite particles. In addition, as a drug carrier, its adsorption behavior of drug and in vitro release kinetics were investigated. Meanwhile, the adsorption kinetic equation of loaded drug and the mechanism of release drug were evaluated.

2. Materials and Methods

2.1. Chemicals. Polyethyleneimine (abbreviated as PEI, M_w 1800 Da), (3-aminopropyl)triethoxysilane (APTES), calcium chloride ($CaCl_2$), sodium carbonate (Na_2CO_3), disodium hydrogen phosphate (Na_2HPO_4), sodium hydroxide (NaOH), sodium dodecyl sulfonate (SDS), dimethyl sulfoxide (DMSO), N,N-dimethylformamide (DMF), folic acid (folate, FA), dicyclohexylcarbodiimide (DCC), and N-hydroxysuccinimide (NHS) were purchased from Sinopharm Chemical Reagent Co., Ltd. (Shanghai). Doxorubicin hydrochloride salt (DOX) was obtained from TaizhouShenxin United Co. Ltd. (China). All other chemicals used in the study were of analytical grade and obtained from commercial sources and the water in the experiment used was distilled for two times.

2.2. Preparation of FA-Grafted Hollow Hydroxyapatite Microspheres. First, the hollow vaterite $CaCO_3$ microspheres were prepared similar to the previous report with proper modifications [43, 44], described in detail as follows: 5mL of PEI (1%) and SDS ($0.015 mol \cdot L^{-1}$) were separately poured into 50 mL of $CaCl_2$ solution ($0.1\ mol \cdot L^{-1}$) under vigorous magnetic stirring, after 10 minutes, 50mL of Na_2CO_3 solution ($0.1\ mol \cdot L^{-1}$) was added dropwise into the above mixed solution, the mixture was heated to 40°C under continuous agitation and kept for 2 h, the white suspension obtained was centrifuged for 5 min at 5000rpm, and the sample was washed with distilled water and then placed in the oven and dried at 80°C for 24 h. Next, the as-obtained $CaCO_3$ 0.1g was dispersed in 50mL distilled water and raised temperature to 60°C after ultrasound for 10min, and then 50mL of Na_2HPO_4 solution (0.03mol·L) was added with the rate of $1.5\ mL \cdot min^{-1}$ under stirring at 400rmp. After that, the pH of the reaction system was adjusted to 11 using NaOH solution and reacted persistently for 2 h. The suspension centrifuged was washed and dried at 65°C for 24h.

The fabricated 0.2 g of hydroxyapatite was dispersed in 100 mL of the solution corresponding to a ratio of absolute ethanol to distilled water 1:1 (volume ratio), the suspension was agitated for 30 min with a magnetic stirrer at room temperature, and then 0.18 g of APTES was added dropwise. After the continuous reaction for 24 h at room temperature, an aminated hydroxyapatite was obtained. The centrifugate was washed adequately enough with absolute ethanol, dried under vacuum, and added to the activated folic acid solution, which was prepared that 0.2g FA was dissolved in DMF/DMSO (28 mL 3: 1) solution contained 0.062g DCC and 0.032g NHS with stirring for 4 h. The generated mixture was reacted with N_2 protection in the dark for 24 hat room temperature. The centrifuged product was washed with water and absolute ethanol and freeze dried, FA-grafted porous hollow hydroxyapatite microspheres were obtained.

2.3. Loading and In Vitro Release of Drug. The adsorption test of DOX on the as-fabricated hydroxyapatite and FA-grafted hydroxyapatite was carried out as follows: 5mg hydroxyapatite and FA-grafted hydroxyapatite were separately added into 50mL DOX solution with different initial concentration. The adsorption has taken place in an orbital shaker at 37°C. At designated time intervals, 3ml of the suspension was separated by centrifuging at 12000rpm for 20min, and the DOX concentration was determined from the supernatant by UV spectrophotometer at a wavelength of 480nm, and the sediment was returned to the adsorption system. The amount of adsorbed DOX q(mg/g) was calculated according to

$$q = \frac{(c_0 - c_e)\, V}{G} \tag{1}$$

where G(g) is the adsorbent material quantity and c_0(mg/L) and c_e(mg/L) are the initial and equilibrium concentrations of DOX in the solution, respectively. V(L) is the solution volume. The influence of adsorption time was monitored for each material. The microspheres of maximum adsorption of drug was dried under vacuum at ambient temperature and stored until use.

As the in vitro drug releases, the drug-loaded microspheres, 10 mg, were placed in dialysis tube (MWCO

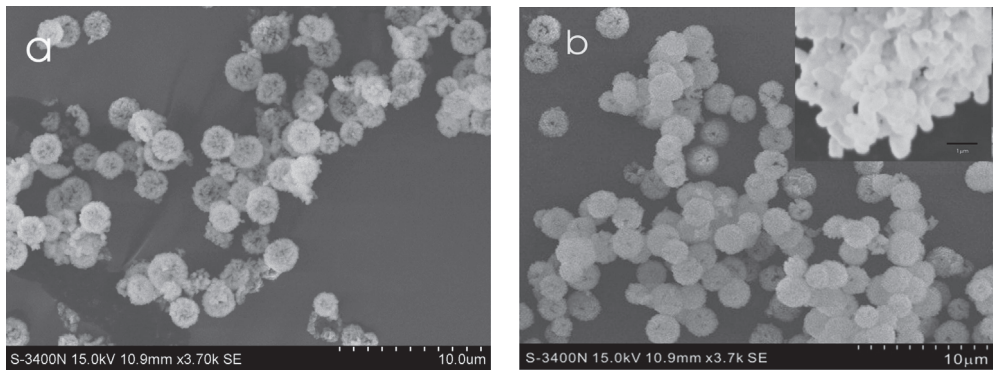

(a) (b)

Figure 1: SEM images of the as-prepared microspheres, (a) hydroxyapatite, and (b) FA-grafted hydroxyapatite.

12-14kDa) and immersed in 25 mL of phosphate buffer solutions (PBS, pH=5.7 or 7.4) and shaken with the constant 200rpm at 37°C. The released solution (2 mL) was removed at fixed time intervals and analyzed the DOX concentration with a UV spectrophotometer at a wavelength of 233 nm, and then the same volume of fresh PBS medium was added to the release system. The released percentage of drug was calculated and the kinetics of release for the drug-loaded FA-grafted hydroxyapatite were investigated in the PBS solution with pH 5.7 and 7.4.

2.4. Characterization. The morphology of the FA-grafted hydroxyapatite was observed by Scanning electron microscopy (SEM, Hitachi S-3400N) at an accelerating voltage of 5-10 kV. Powder X-ray diffraction patterns (X/Pert Pro 3040/60) were used to analyze the structural phase composition with Cu Kαradiation at 40kV and 40mA. Meanwhile, nitrogen adsorption-desorption isotherms were obtained with an surface area and porosity analyzer (ASAP 2020HD88, Micromeritics), after the sample was degassed under vacuum at 80°C for 12 h. Fourier transform infrared (FTIR) spectra were carried out on a Thermo Nicolet 6700 spectrometer with the KBr method. UV-vis absorption measurements were carried out with a Shimadzu UV- 360 spectrophotometer. Thermogravimetric analysis (TGA) was conducted in a TA instrument SDT Q600 with a heating rate of 10°C·min^{-1} under N_2 atmosphere. The diameter size distribution of the samples was determined using a Zetasizer Nano-ZS90 dynamic light scattering instrument. Raman of the sample was measured using the Raman microspectrometer (DXR ThermoFisher) with an excitation wavelength of 532 nm.

3. Results and Discussion

3.1. Morphological and Composition Characteristics. The SEM images of the as-prepared hydroxyapatite and FA-grafted hydroxyapatite are shown in Figure 1. A uniform spherical morphology can be clearly observed, and some broken shapes with hollow interior indicate that the as-prepared microspheres have a porous hollow structure, and the average diameters are around 2.0 μm. From the dynamic light scattering measurement, the mean size of the hydroxyapatite is 2034 nm with PDI (polydispersity index) value of 0.173 and the FA-grafted hydroxyapatite is 2063 nm with PDI of 0.157, respectively. These results are well consistent with the SEM observation, and the porous structure of FA-grafted hydroxyapatite has not been significantly altered (seen in Figure 1(b)). Furthermore, the local magnification image shows that the short rod-shaped microparticles of about 400 nm compose the hollow shape, which is in accord with related research [45, 46].

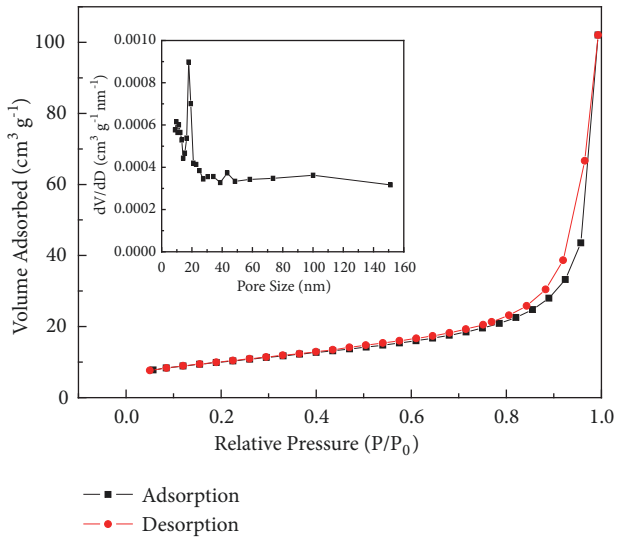

Figure 2: Nitrogen adsorption-desorption isotherms and pore size distribution of the FA-grafted hydroxyapatite.

The nitrogen adsorption/desorption isotherms and the corresponding Barrett–Joyner–Halenda (BJH) pore size distribution is displayed in Figure 2. Clearly, the curve is classified as a type IV isotherm with a hysteresis loop, and the specific surface area of Brunauer-Emmett-Teller (BET) is 34.58m^2/g, the cumulative pore volume is 0.17cm^3/g, and the average pore size is 17.80 nm. By contrast, the hydroxyapatite is assigned severally to 35.07m^2/g, 0.18cm^3/g and 18.89nm. The BET data of the FA-grafted hydroxyapatite do not create a significant difference, also illustrating that the FA grafting

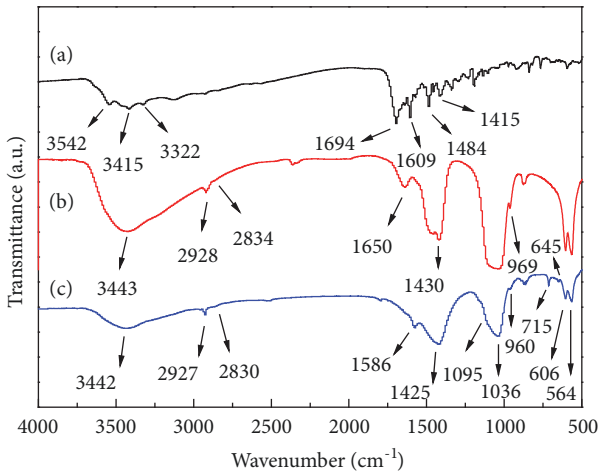

Figure 3: FTIR spectra of the samples. (a) FA; (b) aminated hydroxyapatite; (c) FA-grafted hydroxyapatite.

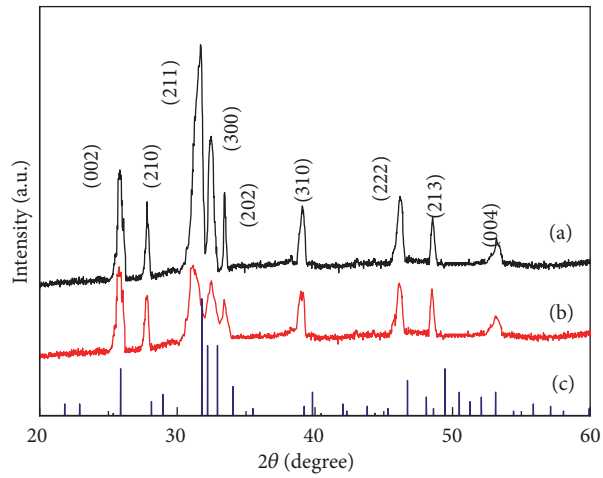

Figure 4: XRD patterns of the samples. (a) FA-grafted hydroxyapatite; (b) aminated hydroxyapatite; (c) hexagonal hydroxyapatite standard card No. 09–0432.

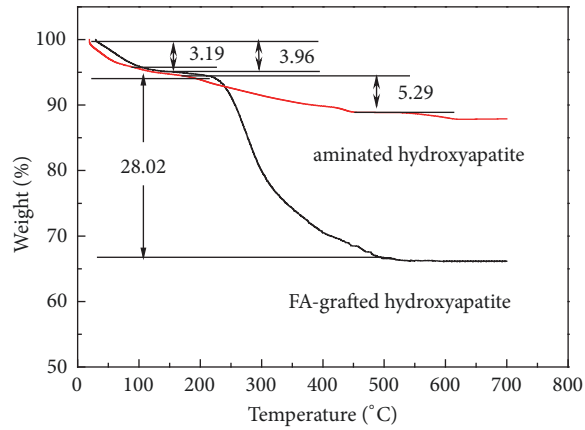

Figure 5: TGA curves of the aminated and FA-grafted hydroxyapatite.

did not alter the porous hollow structure of the as-prepared sample. The porous and hollow structures of the FA-grafted hydroxyapatite are favorable for drug loading and release because they provide the ideal physical space.

Figure 3 shows the FTIR spectrum of the FA-grafted hydroxyapatite, in comparison with FA and aminated hydroxyapatite. In Figure 3(c), the characteristic adsorption peaks at 564 cm^{-1} and 606 cm^{-1} are attributed to the triply degenerated vibration of P–O–P bond in PO_4^{3-} groups, and the intense absorption bands at 1095 cm^{-1} and 1036 cm^{-1} are assigned to the antisymmetric stretching vibration of P–O bond, while the weak peak at 960 cm^{-1} belongs to symmetric stretching of P–O bond. The obviously broad band at 3442 cm^{-1} is related to the overlap for the symmetric stretching of OH (around 3570 cm^{-1}) and adsorbed water. In addition, the adsorption peaks at 2927 cm^{-1} and 2830cm^{-1} are ascribed to the symmetric and asymmetric stretching of CH_2 groups, and the CH_2 deformation vibration is also observed at 1425 cm^{-1}. As the bands observed at 2928, 2834, and 1430 cm^{-1} as well as 969 cm^{-1} in Figure 3(b), in comparison of the corresponding peaks in Figure 3(c), these peaks are shifted to the lower wave numbers, indicating that a certain influence was created due to the FA introduced. It is worth noting that the intense band located at 1650 cm^{-1} of NH_2 in the aminated sample has not been found in Figure 3(c). Instead, a characteristic bending vibration (CNH) of amide II, arising from the amidation between COOH and NH_2, is observed at 1586 cm^{-1}. Furthermore, the band at 645 cm^{-1} results from the bending vibration of O=C-N, and the band at 715 cm^{-1} is ascribed to the out-of-plane bending vibration of N-H. As Raman spectrum of the FA-grafted hydroxyapatite (see Figure S1 in the Supplementary Material for comprehensive image analysis), the special signals correspond to the symmetric bending (ν_2) and stretching (ν_1) vibration as well as the antisymmetric bending (ν_4) and stretching (ν_3) modes of the PO_4^{3-} coincident with the reported work [47, 48]. The stretching vibration of C=O (amide II) especially appears at 1616 cm^{-1}, and the bands at 1582, 664 and 712 cm^{-1} belong to the bending mode (CNH) of amide II, the bending mode of O=C-N, and the out-of-plane bending mode of N-H, respectively. These results are consistent with the analysis of IR and also illustrate to form hydroxyapatite and achieve the grafting of FA onto hydroxyapatite.

X-ray diffraction patterns of the aminated and FA-grafted hydroxyapatite is presented in Figure 4. In contrast to the hexagonal hydroxyapatite (JCPDS card No. 09–0432), all the featured planes can be well indexed, and no other planes of crystalline phase were detected, hinting that the as-prepared samples have a better crystallinity.

Thermal stability analysis of the as-prepared samples was carried out, as shown in Figure 5. The weight losses of 3.19% and 3.96% below 128°C were attributed to evaporation of residual water in the two samples, respectively. The aminated sample created the weight loss of 5.29% at 198–389°C, while in the curve of the FA-grafted hydroxyapatite the sharp weight loss of 28.02% at 245–490°C was due to the decomposition of carbodiimide compounds formed on the surface of the

Table 1: The fitted results of k_1 and k_2 and correlation coefficients for two models.

	FA-grafted hydroxyapatite				Hydroxyapatite			
	Pseudo-first-order		Pseudo-second-order		Pseudo-first-order		Pseudo-second-order	
	$k_1 \times 10^{-4}$ /min^{-1}	R^2	$k_2 \times 10^{-4}$/ L·mg^{-1}·min^{-1}	R^2	$k_1 \times 10^{-4}$/min^{-1}	R^2	$k_2 \times 10^{-5}$/ L·mg^{-1}·min^{-1}	R^2
10 mg/L	9.323	0.9768	1.552	0.9676	2.692	0.9380	3.040	0.9267
15 mg/L	8.534	0.7514	0.9560	0.6494	3.896	0.9653	3.006	0.9737
20mg/L	9.254	0.8813	0.8257	0.7898	3.465	0.9929	1.997	0.9917
25mg/L	9.243	0.9517	0.6295	0.9149	3.260	0.9891	1.501	0.9915

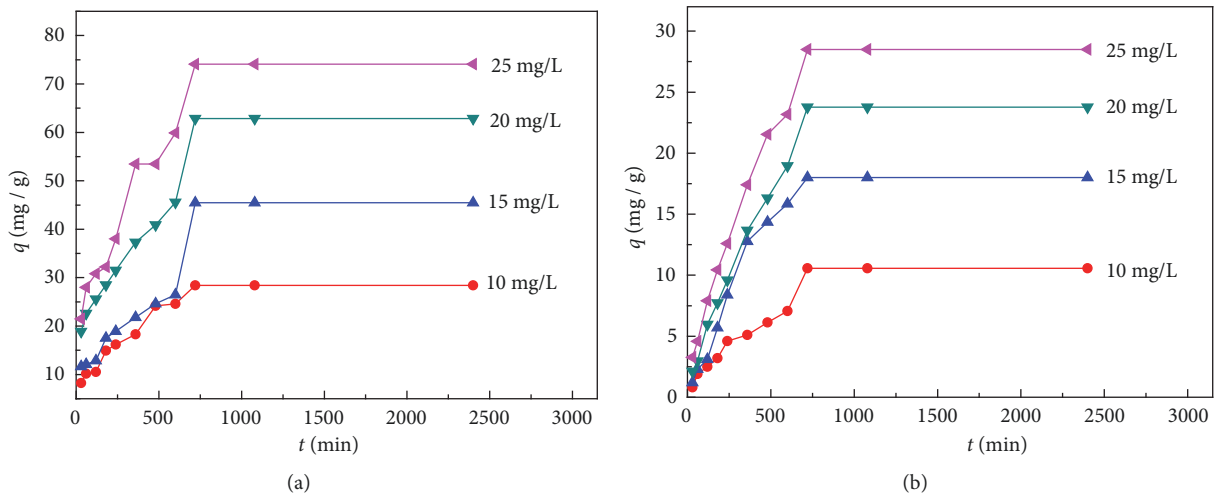

Figure 6: Adsorption capacity of the samples at the various drug concentrations as a function of time. (a) FA-grafted hydroxyapatite; (b) hydroxyapatite.

as-prepared sample, so implying that the grafted results of folic acid resulted in around 22.73% mass loss.

3.2. Adsorption Kinetics. Adsorption capacity of drug on the FA-grafted hydroxyapatite as a function of time is shown in Figure 6(a). One can find that the amount of adsorbed drug increases with the increase of initial DOX concentration, and an adsorption plateau was observed after the adsorption for 12h. As compared with the hydroxyapatite, in Figure 6(b), at the same drug concentration and time, the adsorption capacity of the former was 2–3 times as much as the latter, revealing that the adsorption rate was the same multiple of the latter. In other words, the adsorption performance of the FA-grafted hydroxyapatite is far better than that of the hydroxyapatite. According to the specific surface measuring of the FA-grafted hydroxyapatite and the hydroxyapatite, their values have no prominent difference; hence, the specific surface is not a main factor for leading to the apparent difference in adsorption capacity. For the as-prepared FA-grafted hydroxyapatite with porous hollow structure, a lot of carboxyl groups exist on the surface of the porous microspheres, and these groups may create strong interaction with the amino in the DOX molecule. However, as the unfunctionalized hydroxyapatite, the OH groups in porous hollow hydroxyapatite can only provide relatively low affinity towards the drug molecules. Therefore, the FA-grafted hydroxyapatite shows a higher adsorption capacity and rate at the same concentration. As for the jumps of adsorption capacity for both the samples between 500 and 1000 mints, the more possible reason arises from the physical adsorption at later stage of adsorption.

To confirm the kinetic equation of adsorption process of drug, the classical pseudo-first-order and pseudo-second-order kinetic model are used, and the model equations are as follows:

$$-\ln c = k_1 t - \ln c_0 \tag{2}$$

$$\frac{1}{c} = k_1 t + \frac{1}{c_0} \tag{3}$$

where c (mg/L) and c_0 (mg/L) are assigned severally to the solution concentration of drug at time t and the initial concentration, and k_1(min^{-1}) and k_2(L·mg^{-1}·min^{-1}) are the rate constant of corresponding model equation. The calculated results are listed in Table 1. As compared to k_2, one can see that k_1 of the FA-grafted hydroxyapatite is close to not only a constant but also the hydroxyapatite. In the meantime, the values of correlation coefficient associated with the pseudo-first-order are better than that of the pseudo-second-order except for the individual R^2 of the hydroxyapatite; it means that the adsorbed behavior of drug on the adsorbents is more suitable to be described with the pseudo-first-order model.

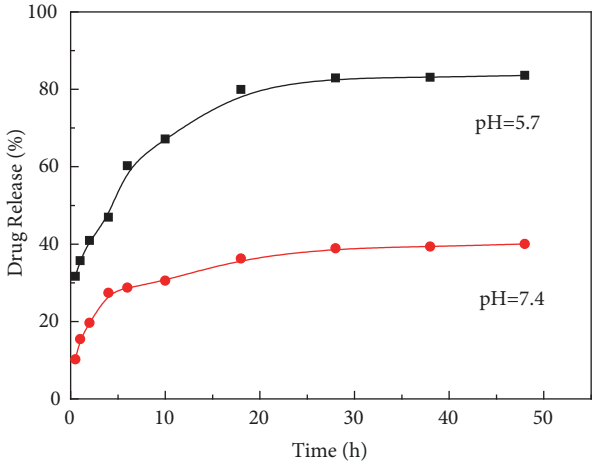

Figure 7: The release curves of DOX-loaded FA-grafted hydroxyapatite in PBS at pH 5.7 and 7.4.

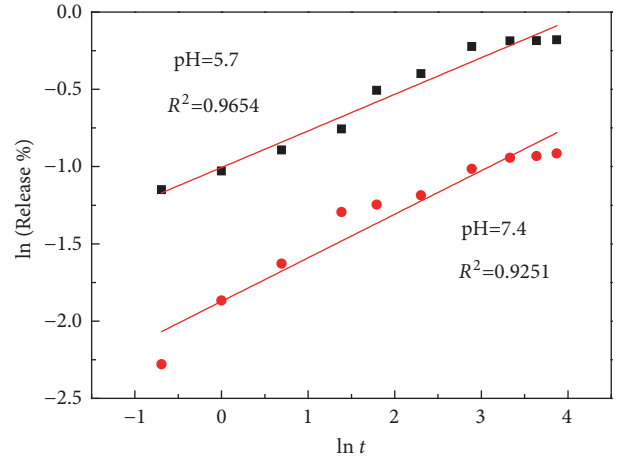

Figure 8: Natural logarithm of the release fraction of drug as a function of ln t.

3.3. Drug Release. The releases of the DOX-loaded FA-grafted hydroxyapatite in PBS solution are plotted in Figure 7. It can be found that both of the DOX releases at pH value of 5.7 and 7.4 at 37°C exhibited a similar trend, and the release plateaus were all reached after 28 hours, indicating that the drug-loaded FA-grafted hydroxyapatite showed a slow and sustained release behavior. Meanwhile, nearly 83% of the loaded DOX was released in the PBS solution with pH 5.7. This amount of release was higher than that of the approximately 39% in the PBS solution with pH 7.4, implying that the DOX-loaded FA-grafted hydroxyapatite had a pH-responsive characteristic for controlling release. This pH-responsive release was mainly attributed to the higher solubility of the DOX-loaded FA-grafted hydroxyapatite in PBS solution with a low pH value than that in PBS with a high pH value. Certainly, the interaction decreasing between DOX molecular and the carriers due to the protonation of the amino and carboxyl groups in the acidic PBS solution may play partly a role. It is worth noting that, in the PBS solution with pH 5.7, the DOX-loaded FA-grafted hydroxyapatite underwent a rapid release in the first 6 h, while in the PBS solution with pH 7.4 the rapid release was about in the first 4 h; after that, a slow release was all displayed in the range of next time to 48 h. It revealed that the as-prepared FA-grafted hydroxyapatite has excellent controlled-release property of drug. In the initial stage of the DOX release, the DOX molecules adsorbed close to the surface diffused easily into the bulk solution, and then the DOX molecules, which was bound to the FA-grafted hydroxyapatite matrix and located below the surface, performed to diffuse through the FA-grafted hydroxyapatite matrix and pores in the matrix, so in this case a slow and sustain-controlled release was observed.

The drug, DOX, is loaded into the porous hollow hydroxyapatite through the adsorption pathway, and the drug release may be regarded as a liking release behavior of matrix system. Hence, Korsmeyer-Peppas mathematical model can be used to analyze the mechanism of the drug release. The model equation is [49]

$$\frac{M_t}{M_\infty} = at^n \tag{4}$$

where M_t/M_∞ is the fraction of drug release at time t, and a is the release rate constant, and n is the release exponent. The experimental data obtained from in vitro drug release are linearly fitted in Figure 8. In terms of the calculated results, the correlation coefficients, R^2, are 0.9654 and 0.9251 in the PBS solution with pH 5.7 and 7.4, respectively, and the n values are correspondingly 0.24 and 0.28. The high R^2 value hints a good correlation degree which is well consistent with Korsmeyer-Peppas model. The value of n is all less than 0.5, indicating that the process of drug release belongs to Fickian diffusion mechanism.

As for Fickian diffusion second law, the overall process of release in a certain thickness device can be divided into early and late stage, and in the early stage the release amount is proportional to the square root of time, whereas in the late stage the release amount is an exponential function of time due to the decrease of drug concentration in the device. Therefore, when the release rate data in the initial stage are taken the natural logarithm and plotted against ln$t$ and the slope of the fitted straight line should be 0.5. Thereupon the related release data were analyzed, as shown in Figure 9; the high values of R^2 are all obtained, and at pH 7.4 the slope is 0.4609; it is nearly 0.5; that is, the release behavior accords with Fickian second law. Meanwhile, the slope is only 0.2547 at pH 5.7; there is a larger difference value than 0.5, implying that the release did not well conform to Fickian second law. This might be attributed to the dissolution of the loaded drug in the low pH condition, which led to a little anomalous behavior of drug diffusion in the first 6 hours.

4. Conclusions

SEM and the relevant characterizations have demonstrated that the FA-grafted hydroxyapatite microspheres with porous hollow structure were successfully prepared, and FA grafted onto the surface of modified hydroxyapatite did not alter the porous hollow structure of the as-prepared hydroxyapatite.

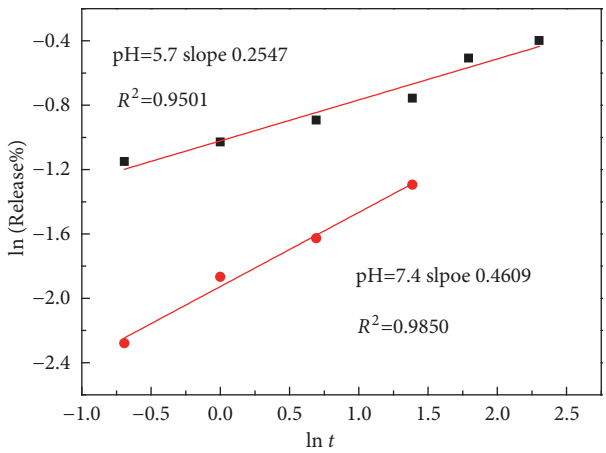

Figure 9: Natural logarithm of the drug release rate as a function of ln$t$ in the early stage of drug release.

For the loading of drug DOX, the FA-grafted hydroxyapatite showed a higher loading capacity compared to the hydroxyapatite due to the strong interaction between the carboxyl group on the surface of FA-grafted microspheres and the amino in the DOX molecule, and the adsorption kinetics of drug for the two microspheres are well consistent with pseudo-first-order model. The drug release of the DOX-loaded FA-grafted microspheres in the solution of pH 5.7 and pH 7.4 showed a rapid release in the initial stage and then sustained release in the next time, revealing that an excellent property of pH-controlled release, and the release behavior could be well described with Korsmeyer-Peppas mathematical model and fitted in with Fickian diffusion second law.

Data Availability

The related spectrum and testing data used to support the findings of this study are available from the corresponding author upon request.

Conflicts of Interest

The authors declare that there are no conflicts of interest regarding the publication of this paper.

Acknowledgments

This work has been financially supported by the National Natural Science Foundation of China (no. 21672151) and Collaborative Innovation Fund of Shanghai institute of technology (no. 39120K178030).

Supplementary Materials

Figure S1: Raman spectrum of the FA-grafted hydroxyapatite. *(Supplementary Materials)*

References

[1] A. Pangon, S. Saesoo, N. Saengkrit, U. Ruktanonchai, and V. Intasanta, "Hydroxyapatite-hybridized chitosan/chitin whisker-bionanocomposite fibers for bone tissue engineering applications," *Carbohydrate Polymers*, vol. 144, no. 25, pp. 419–427, 2016.

[2] D. L. Batchelar, M. T. M. Davidson, W. Dabrowski, and I. A. Cunningham, "Bone composition imaging using coherent-scatter computed tomography: assessing bone health beyond bone mineral density," *Medical Physics*, vol. 33, no. 4, pp. 904–915, 2006.

[3] L. H. Li, K. P. Kommareddy, C. Pilz, C. R. Zhou, P. Fratzl, and I. Manjubala, "In vitro bioactivity of bioresorbable porous polymeric scaffolds incorporating hydroxyapatite microspheres," *Acta Biomaterialia*, vol. 6, no. 7, pp. 2525–2531, 2010.

[4] S. Pujari-Palmer, S. Chen, S. Rubino et al., "In vivo and in vitro evaluation of hydroxyapatite nanoparticle morphology on the acute inflammatory response," *Biomaterials*, vol. 90, pp. 1–11, 2016.

[5] A. Rabiei, T. Blalock, B. Thomas, J. Cuomo, Y. Yang, and J. Ong, "Microstructure, mechanical properties, and biological response to functionally graded HA coatings," *Materials Science and Engineering C: Materials for Biological Applications*, vol. 27, no. 3, pp. 529–533, 2007.

[6] L. Chen, J. M. Mccrate, J. C. Lee, and H. Li, "The role of surface charge on the uptake and biocompatibility of hydroxyapatite nanoparticles with osteoblast cells," *Nanotechnology*, vol. 22, article 105708, no. 10, 2011.

[7] E. Ahmadzadeh, F. Talebnia, M. Tabatabaei, H. Ahmadzadeh, and B. Mostaghaci, "Osteoconductive composite graft based on bacterial synthesized hydroxyapatite nanoparticles doped with different ions: From synthesis to in vivo studies," *Nanomedicine: Nanotechnology, Biology and Medicine*, vol. 12, no. 5, pp. 1387–1395, 2016.

[8] D. Tsiourvas, A. Sapalidis, and T. Papadopoulos, "Hydroxyapatite/chitosan-based porous three-dimensional scaffolds with complex geometries," *Materials Today Communications*, vol. 7, pp. 59–66, 2016.

[9] V. Sarath Chandra, G. Baskar, R. V. Suganthi et al., "Blood compatibility of iron-doped nanosize hydroxyapatite and its drug release," *ACS Applied Materials & Interfaces*, vol. 4, no. 3, pp. 1200–1210, 2012.

[10] P. P. Yang, Z. W. Quan, C. X. Li, X. J. Kang, H. Z. Lian, and J. Lin, "Bioactive, luminescent and mesoporous europium-doped hydroxyapatite as a drug carrier," *Biomaterials*, vol. 29, no. 32, pp. 4341–4347, 2008.

[11] S. Leprêtre, F. Chai, J.-C. Hornez et al., "Biomaterials prolonged local antibiotics delivery from hydroxyapatite functionalized with cyclodextrin polymers," *Biomaterials*, vol. 30, no. 30, pp. 6086–6093, 2009.

[12] C. Santos, C. F. Rovath, R.-P. Franke, M. M. Almeida, and M. E. V. Costa, "Spray-dried hydroxyapatite-5-Fluorouracil granules as a chemotherapeutic delivery system," *Ceramics International*, vol. 35, no. 1, pp. 509–513, 2009.

[13] Y. Chen, L. Yang, S. Huang, Z. Li, L. Zhang, J. He et al., "Delivery system for DNAzymes using arginine-modified hydroxyapatite nanoparticles for therapeutic application in a nasopharyngeal carcinoma model," *International Journal of Nanomedicine*, vol. 8, pp. 3107–3118, 2013.

[14] S. Sarda, F. Errassifi, O. Marsan, A. Geffre, C. Trumel, and C. Drouet, "Adsorption of tranexamic acid on hydroxyapatite:

toward the development of biomaterials with local hemostatic activity," *Materials Science and Engineering C: Materials for Biological Applications*, vol. 66, pp. 1–7, 2016.

[15] Y. Lu and P. S. Low, "Folate-mediated delivery of macromolecular anticancer therapeutic agents," *Advanced Drug Delivery Reviews*, vol. 54, no. 5, pp. 675–693, 2002.

[16] R. Cheng, F. H. Meng, C. Deng, H. A. Klok, and Z. Y. Zhong, "Dual and multi-stimuli responsive polymeric nanoparticles for programmed site-specific drug delivery," *Biomaterials*, vol. 34, no. 14, pp. 3647–3657, 2013.

[17] J. Pan, D. Wan, Y. Bian et al., "Fluorescent hydroxyapatite-loaded biodegradable polymer nanoparticles with folate decoration for targeted imaging," *AIChE Journal*, vol. 59, no. 12, pp. 4494–4501, 2013.

[18] A. Ashokan, D. Menon, S. Nair, and M. Koyakutty, "A molecular receptor targeted, hydroxyapatite nanocrystal based multimodal contrast agent," *Biomaterials*, vol. 31, no. 9, pp. 2606–2616, 2010.

[19] S. S. Syamchand, S. Priya, and G. Sony, "Hydroxyapatite nanocrystals dually doped with fluorescent and paramagnetic labels for bimodal (luminomagnetic) cell imaging," *Microchimica Acta*, vol. 182, no. 5-6, pp. 1213–1221, 2015.

[20] G. D. Venkatasubbu, S. Ramasamy, G. S. Avadhani, V. Ramakrishnan, and J. Kumar, "Surface modification and paclitaxel drug delivery of folic acid modified polyethylene glycol functionalized hydroxyapatite nanoparticles," *Powder Technology*, vol. 235, pp. 437–442, 2013.

[21] A. K. Sánchez Lafarga, F. P. Pacheco Moisés, A. Gurinov, G. G. Ortiz, and G. G. Carbajal Arízaga, "Dual responsive dysprosium-doped hydroxyapatite particles and toxicity reduction after functionalization with folic and glucuronic acids," *Materials Science and Engineering C: Materials for Biological Applications*, vol. 48, pp. 541–547, 2015.

[22] M. F. Cipreste, I. Gonzalez, T. Maria Da Mata Martins, A. M. Goes, W. Augusto De Almeida Macedo, and E. M. Barros De Sousa, "Attaching folic acid on hydroxyapatite nanorod surfaces: an investigation of the HA–FA interaction," *RSC Advances*, vol. 6, no. 80, pp. 76390–76400, 2016.

[23] M. Iafisco, B. Palazzo, T. Ito et al., "Preparation of core-shell poly(L-lactic) acid-nanocrystalline apatite hollow microspheres for bone repairing applications," *Journal of Materials Science: Materials in Medicine*, vol. 23, no. 11, pp. 2659–2669, 2012.

[24] G. J. Owens, R. K. Singh, F. Foroutan et al., "Sol-gel based materials for biomedical applications," *Progress in Materials Science*, vol. 77, pp. 1–79, 2016.

[25] L. Hao, H. Yang, S. Du, N. Zhao, and Y. Wang, "The growth process of hierarchical porous hydroxyapatite microspheres precipitated by propionamide and citrate through hydrothermal synthesis," *Materials Letters*, vol. 131, pp. 252–254, 2014.

[26] Q. Zhong, W. Li, X. Su et al., "Degradation pattern of porous $CaCO_3$ and hydroxyapatite microspheres in vitro and in vivo for potential application in bonetissue engineering," *Colloids and Surfaces B: Biointerfaces*, vol. 143, pp. 56–63, 2016.

[27] K. Lin, P. Liu, L. Wei et al., "Strontium substituted hydroxyapatite porous microspheres: Surfactant-free hydrothermal synthesis, enhanced biological response and sustained drug release," *Chemical Engineering Journal*, vol. 222, pp. 49–59, 2013.

[28] K. Lin, X. Liu, J. Chang, and Y. Zhu, "Facile synthesis of hydroxyapatite nanoparticles, nanowires and hollow nano-structured microspheres using similar structured hard-precursors," *Nanoscale*, vol. 3, no. 8, pp. 3052–3055, 2011.

[29] H. Chen and S. Leng, "Rapid synthesis of hollow nanostructured hydroxyapatite microspheres via microwave transformation method using hollow $CaCO_3$ precursor microspheres," *Ceramics International*, vol. 41, no. 2, pp. 2209–2213, 2015.

[30] C. Qi, Y.-J. Zhu, B.-Q. Lu et al., "Hydroxyapatite hierarchically nanostructured porous hollow microspheres: Rapid, sustainable microwave-hydrothermal synthesis by using creatine phosphate as an organic phosphorus source and application in drug delivery and protein adsorption," *Chemistry - A European Journal*, vol. 19, no. 17, pp. 5332–5341, 2013.

[31] Y. Jiao, Y.-P. Lu, G.-Y. Xiao, W.-H. Xu, and R.-F. Zhu, "Preparation and characterization of hollow hydroxyapatite microspheres by the centrifugal spray drying method," *Powder Technology*, vol. 217, pp. 581–584, 2012.

[32] M.-J. Kim and Y.-H. Koh, "Synthesis of aligned porous poly(ε-caprolactone) (PCL)/hydroxyapatite (HA) composite microspheres," *Materials Science and Engineering C: Materials for Biological Applications*, vol. 33, no. 4, pp. 2266–2272, 2013.

[33] J. S. Son, M. Appleford, J. L. Ong et al., "Porous hydroxyapatite scaffold with three-dimensional localized drug delivery system using biodegradable microspheres," *Journal of Controlled Release*, vol. 153, no. 2, pp. 133–140, 2011.

[34] J. Ma and J. Qin, "Graphene-like zinc substituted hydroxyapatite," *Crystal Growth and Design*, vol. 15, no. 3, pp. 1273–1279, 2015.

[35] Y. Hu, S. Ma, Z. Yang et al., "Facile fabrication of poly(L-lactic acid) microsphere-incorporatedcalcium alginate/hydroxyapatite porous scaffolds based on Pickering emulsion templates," *Colloids and Surfaces B: Biointerfaces*, vol. 140, pp. 382-291, 2016.

[36] Y. Yu, Y. Zhu, C. Qi, Y. Jiang, H. Li, and J. Wu, "Hydroxyapatite nanorod-assembled porous hollow polyhedral as drug/protein carriers," *Journal of Colloid and Interface Science*, vol. 496, pp. 416–424, 2017.

[37] S. Mondal, S. V. Dorozhkin, and U. Pal, "Recent progress on fabrication and drug delivery applications of nanostructured hydroxyapatite," *WIREs Nanomed Nanobiotechnol*, vol. 1, pp. 1–32, 2017.

[38] M. R. Mohammadi, A. Nojoomi, M. Mozafari, A. Dubnika, M. Inayathullah, and J. Rajadas, "Nanomaterials engineering for drug delivery: a hybridization approach," *Journal of Materials Chemistry B*, vol. 5, no. 22, pp. 3995–4018, 2017.

[39] A. Galbiati, C. Tabolacci, B. Morozzo Della Rocca et al., "Targeting tumor cells through chitosan-folate modified microcapsules loaded with camptothecin," *Bioconjugate Chemistry*, vol. 22, no. 6, pp. 1066–1072, 2011.

[40] Y. Zhu, Y. Fang, and S. Kaskel, "Folate-conjugated Fe3O4@SiO2 hollow mesoporous spheres for targeted anticancer drug delivery," *The Journal of Physical Chemistry C*, vol. 114, no. 39, pp. 16382–16388, 2010.

[41] S. I. U. Madrid, U. Pal, Y. S. Kang, J. Kim, H. Kwon, and J. Kim, "Fabrication of Fe3O4@mSiO2 core-shell composite nanoparticles for drug delivery applications," *Nanoscale Research Letters*, vol. 10, pp. 217–224, 2015.

[42] Y. Hu, W. Liu, and F. Wu, "Novel multi-responsive polymer magnetic microgels with folate or methyltetrahydrofolate ligand as anticancer drug carriers," *RSC Advances*, vol. 7, no. 17, pp. 10333–10344, 2017.

[43] V. E. Bosio, M. L. Cacicedo, B. Calvignac et al., "Synthesis and characterization of $CaCO_3$-biopolymer hybrid nanoporous microparticles for controlled release of doxorubicin," *Colloids and Surfaces B: Biointerfaces*, vol. 123, pp. 158–169, 2014.

[44] Y. Pan, X. Zhao, Y. Guo et al., "Controlled synthesis of hollow calcite microspheres modulated by polyacrylic acid and sodium dodecyl sulfonate," *Materials Letters*, vol. 61, no. 13, pp. 2810–2813, 2007.

[45] Y. Sun, Y. Chen, X. Ma et al., "Mitochondria-targeted hydroxyapatite nanoparticles for selective growth inhibition of lung cancer in vitro and in vivo," *ACS Applied Materials & Interfaces*, vol. 8, no. 39, pp. 25680–25690, 2016.

[46] P. Kanchana and C. Sekar, "Development of electrochemical folic acid sensor based on hydroxyapatite nanoparticles," *Spectrochimica Acta Part A: Molecular and Biomolecular Spectroscopy*, vol. 137, pp. 58–65, 2015.

[47] S. Koutsopoulos, "Synthesis and characterization of hydroxyapatite crystals: a review study on the analytical methods," *Journal of Biomedical Materials Research Part B: Applied Biomaterials*, vol. 62, no. 4, pp. 600–612, 2002.

[48] D. Yamini, G. Devanand Venkatasubbu, J. Kumar, and V. Ramakrishnan, "Raman scattering studies on PEG functionalized hydroxyapatite nanoparticles," *Spectrochimica Acta Part A: Molecular and Biomolecular Spectroscopy*, vol. 117, pp. 299–303, 2014.

[49] P. Costa and J. M. Sousa Lobo, "Modeling and comparison of dissolution profiles," *European Journal of Pharmaceutical Sciences*, vol. 13, no. 2, pp. 123–133, 2001.